https://doi.org/10.22226/2410-3535-2023-2-158-163



# Tribological behavior of the electron beam additive manufactured Ti6Al4V-Cu alloy

A. V. Nikolaeva†, A. P. Zykova, A. V. Chumaevskii, A. V. Vorontsov, E. O. Knyazhev, A. V. Nikonenko, S. Yu. Tarasov

†nikolaeva@ispms.ru

Institute of Strength Physics and Materials Science of the SB of the RAS, Tomsk, 634055, Russia

Earlier studies have shown that it is possible to successfully obtain Ti6Al4V-Cu alloys with various copper concentrations using the double-wire electron beam additive manufacturing. Obtaining these alloys is of a practical interest for creating a titanium-base composite material with reduced risk of spontaneous combustion, which could be used in friction units at elevated temperatures. This article presents a study of the tribological properties of Ti6Al4V titanium alloy samples produced by layer-by-layer electron beam melting with the addition of Cu from a wire. The results of this work demonstrate an improved wear resistance of Ti6Al4V-Cu alloys. Such a result was achieved due to the grain refinement and precipitation of intermetallic $Ti_2Cu$ nanosized particles. For instance, the value of linear wear of alloys Ti6Al4V-6 wt.% Cu and Ti6Al4V-9.7 wt.% Cu is 46% and 40% less, respectively, as compared to the original alloy Ti6Al4V. It has been established that the plastic deformation penetration below the worn surface decreases with the increase in the concentration of copper in titanium alloy samples.

**Keywords:** titanium alloys, additive manufacturing, wear resistance, subsurface layer.

## 1. Introduction

The widespread use of titanium alloys in the aviation, rocket and space industries is due to their low specific gravity, high strength, excellent corrosion resistance and high temperature stability [1,2]. Titanium alloys are used in manufacturing of such important and critical parts of aircraft and jet engines as disks, blades and intermediate rings [3] and allow reducing the weight of the product by about half as compared to those made of steel [4]. The use of titanium alloys at high temperatures may be limited by the possibility of their spontaneous combustion caused by high-speed friction in contact with other materials during operation in aircraft engines. The sensitivity of titanium alloys to spontaneous combustion at high temperatures is due to their active chemical properties, high calorific value and low thermal conductivity [5,6]. The combustion process of titanium and its alloys is considered to be a reaction in the liquid phase, i. e. the oxidation of liquid metal [5].

It was found [7] that the addition of Cu increased the combustion resistance of titanium alloys by reducing heat generation and improving their thermal conductivity. The combustion mechanisms of Ti-Cu alloys with different Cu contents (2, 7, 12, 17, 22 wt.%), as well as the formation of the $Ti_2Cu$ phase in various areas of the combustion reaction was reported [7]. In particular, it was reported that both the thickness of the $Ti_2Cu$ layer and volume of the molten $Ti_2Cu$ phase increased with the Cu content. This layer played a role of a diffusion barrier for oxygen and thus allowed reducing the burning rate of titanium alloys.

There are a significant number of methods for obtaining materials resistant to combustion from casting into molds [8] to laser cladding [9]. Currently, there are additive manufacturing methods based on laser [10], arc [11], plasma-arc [12] and electron-beam [13] additive technologies, which include the use of powders or wires as starting materials.

The electron-beam additive manufacturing (EBAM) has a number of advantages in obtaining products from titanium alloys in comparison to other methods. However, there are limitations associated mainly with the formation of coarse-grained structures and, accordingly, with the anisotropy of mechanical properties. Obtaining equiaxed grains can be achieved by adjusting the heat input [14], interlayer working [15], or by introducing alloying elements to expand the zone of constitutional supercooling [16].

Previously, it was found out that the increase in the copper content from 0.6 to 9.7 wt.% in the titanium alloy Ti6Al4V caused a transition from a columnar structure to a columnar-equiaxed and completely equiaxed structure [17]. Thus, when copper is introduced into a titanium alloy, a double effect could have been achieved. On the one hand, it is the enhanced combustion resistance, and on the other hand, the grain refinement and the improvement of mechanical properties. In this regard, wear resistance testing of titanium alloys obtained by the additive method alloyed with copper is of particular interest.

## 2. Materials and experimental method

The additive samples in the form of walls were obtained using an electron-beam additive manufacturing machine (Institute of Strength Physics and Materials Science SB RAS) by layer-by-layer simultaneous deposition from ∅ 1.6 mm Ti6Al4V titanium alloy and ∅ 1 mm C11000 grade copper wires on the Ti grade 2 substrate. A more detailed description

of the double-wire deposition technique is disclosed elsewhere [17]. Depending on the copper concentration in the titanium alloy, three types of composite alloys have been obtained as follows: hypoeutectoid (Ti6Al4V-0.6 wt.% Cu and Ti6Al4V-1.6 wt.% Cu), eutectoid (Ti6Al4V-6 wt.% Cu), and hypereutectoid (Ti6Al4V-9.7 wt.% Cu).

On cutting from the as-manufactured walls the samples have been subjected to standard sample preparation that included grinding, polishing, and etching of the obtained materials with the $HF:HCl:HNO_3:H_2O$ reagent in a ratio of 2:3:4:41. The microstructure of the samples was studied by optical microscopy using a microscope Altami Met 1S, transmission electron microscopy on a JEOL-210 microscope and by scanning electron microscopy (SEM, Thermo Fisher Scientific Apreo S LoVac equipped with an energy dispersive spectrometer (EDS) and an electron backscattered diffraction (EBSD) camera). X-ray diffraction (XRD) studies were carried out on an XRD-7000S diffractometer using $CoK_\alpha$ radiation.

A DM 8 microhardness tester (Affri, Italy, Center for Collective Use NANOTECH, Institute of Physics and Technology, Siberian Branch of the Russian Academy of Sciences) with an indenter load of 50 g, dwell time of 10 s with a step of 0.5 mm was used for measuring the microhardness. Unlubricated sliding friction was carried out on a Tribotester setup according to the "pin-on-disk" scheme (Fig. 1). The sliding test samples had dimensions $3\times3\times10$ mm$^3$ and were made of Ti6Al4V-Cu alloy with different concentrations of copper, so that their worn surfaces were perpendicular to the wall building direction. The counterbodies were made of Ti6Al4V alloy in the form of ∅30 mm disks. The disk rotation

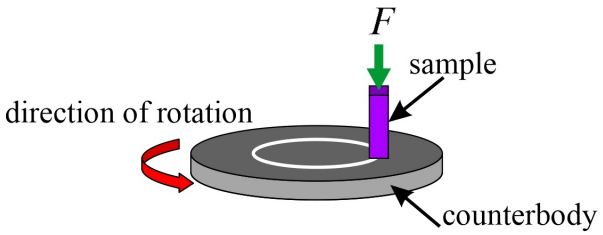


**Fig. 1.** (Color online) Scheme of testing samples of the Ti6Al4V-Cu alloy for wear resistance testing.

frequency was 250 rpm, pin normal load $F$=15 N, test time 2 h. The total length of the sliding path for each sample was $N$=1884 m with a wear track radius of 10 mm.

## 3. Results and discussion

The macrostructure of the Ti6Al4V-0.6 wt.% Cu alloy, obtained by electron-beam additive manufacturing is represented by columnar grains with the average length and width 11.62 ± 5.42 mm and 1.06 ± 0.79 mm, respectively (Fig. 2 a, b). The Ti6Al4V-0.6 wt.% Cu sample is characterized by α + β lamellar structure and Widmannstatten structure with an average length of α-plates 6.31 ± 2.71 μm (Fig. 2 a and c).

With the increase in the concentration of copper from 0.6 to 6 and 9.7 wt.%, the primary β-grains refined and a transition from a columnar structure to the completely equiaxed one occurred. The average grain sizes for alloys Ti6Al4V-6 wt.% Cu and Ti6Al4V-9.7 wt.% Cu are 0.42 ± 0.19 mm and 0.46 ± 0.19 mm, respectively (Fig. 3).

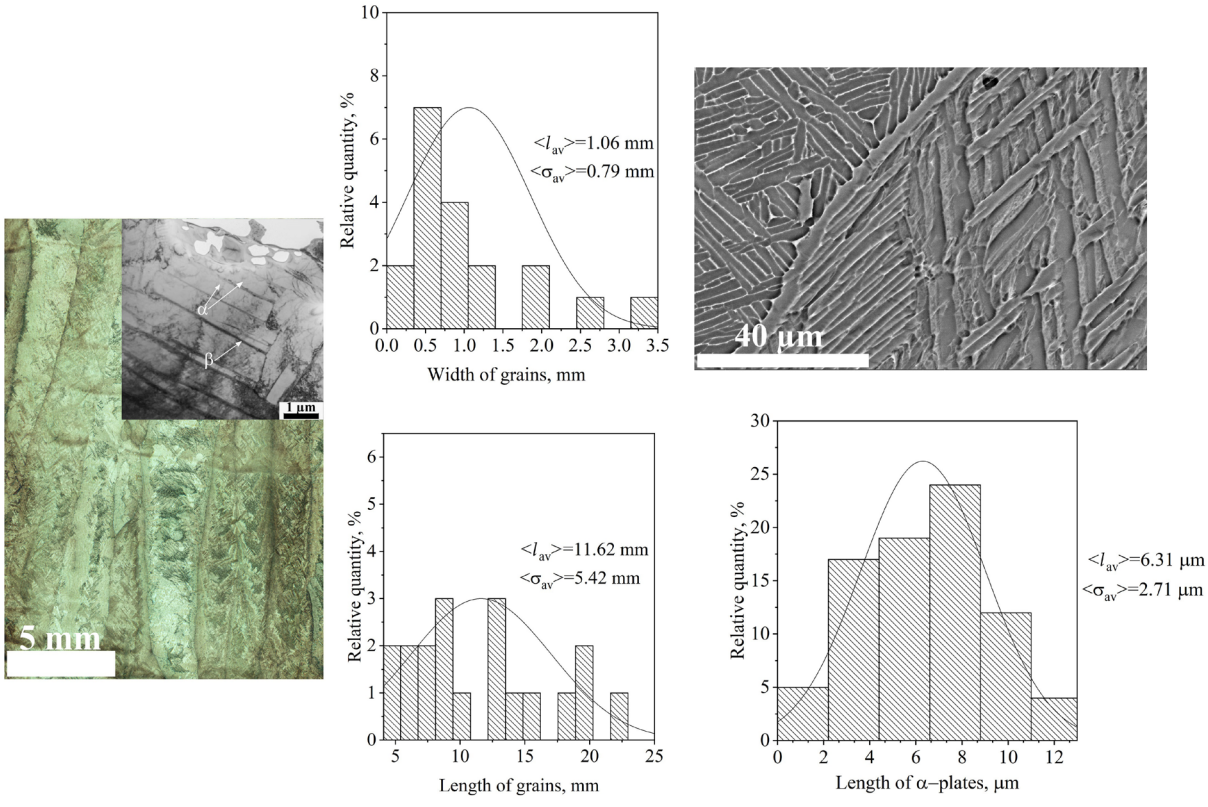


**Fig. 2.** (Color online) Macrostructure (a) and grain size distribution histograms (b), length distribution histogram of α-plates (c) of Ti6Al4V-0.6 wt.% Cu samples obtained by electron-beam additive manufacturing.

The microstructures in TiAl64V-6 wt.% Cu samples as well as both β-grain size distributions (Fig. 3 a) evidence that adding 6 wt.% copper resulted in forming almost equiaxed β-grains with corresponding smaller α-Ti and α'-Ti crystallites. The SEM image of the Ti6Al4V-9.7 wt.% Cu alloy shows that polymorphic transformation $\beta \rightarrow \alpha(\alpha')$ in cooling resulted in forming the α-plates with a length of 50 nm (Fig. 3 b). Previously, using the bright-field TEM images, it was found that $Ti_2Cu$ particles with an average size of 180 nm were distributed in thick boundary layers of the α-phase of the Ti6Al4V-6 wt.% Cu alloy (Fig. 3 a). The α/β colonies of the Ti6Al4V-9.7 wt.% Cu alloy contain nanosized $Ti_2Cu$ particles with the average size 200 nm (Fig. 3 b) [17].

The inverse and direct pole figures were obtained using the EBSD method from the composite alloys Ti6Al4V-0.6 wt.% Cu, Ti6Al4V-6 wt.% Cu and Ti6Al4V-9.7 wt.% Cu (Fig. 4). Typical hexagonal crystal pole figures (0001) and $(10\bar{1}0)$ are shown with only one pole for (0001) plane and three for $(10\bar{1}0)$ plane (Fig. 4 a). The boundaries of the primary columnar β-Ti grains can be observed in the inverse pole figure (Fig. 4 a). Large columnar grains in the Ti6Al4V-0.6 wt.% Cu samples are represented by boundaries, within which α-Ti grains are observed with orientations inside the standard triangle with vertices $[0001][10\bar{1}0]$ and $[2\bar{1}\bar{1}0]$. The large α-Ti grain in the upper part of the inverse pole figure has an orientation close to $[10\bar{1}2]$ and is possibly a β-Ti grain with the original orientation. In samples Ti6Al4V-6 wt.% Cu (Fig. 4 b) and Ti6Al4V-9.7 wt.% Cu (Fig. 4 c) the boundaries of the former large but equiaxed β-Ti grains are clearly visible, inside which small α-Ti grains are observed with different orientations close to those that exist in the Ti6Al4V-0.6 wt.% Cu sample. It should be noted that the distribution of grain orientations in the last two cases is much more diverse, as follows from the direct pole figures Fig. 4.

Figure 5 shows the results of Vickers microhardness measurements for alloys with different copper contents. It can be seen that microhardness grows with the Cu content in the Ti6Al4V due to precipitation of $Ti_2Cu$ particles and hardening of the α-Ti solid solution. The highest values of microhardness were typical for samples Ti6Al4V-6 wt.% Cu ($\langle HV \rangle = 3.9 \pm 0.3$ GPa) and Ti6Al4V-9.7 wt.% Cu ($\langle HV \rangle = 5.4 \pm 0.5$ GPa), which are 34% and 86% higher than the microhardness of Ti6Al4V ($\langle HV \rangle = 2.9 \pm 0.1$ GPa), respectively. The highest values of microhardness for these alloys are due to transition from columnar to equiaxed grains, α-grain refinement, and $Ti_2Cu$.

During the test, the coefficient of friction (COF) was measured so that the obtained COF dependencies on time indicated the presence of an approximately 1000 s running-in period, after which the COF values slightly decreased and then remained constant at the level of 0.3 – 0.34 (Fig. 6). At the same time, some difference in the COF values among the samples was observed by their running-in periods.

To quantize the wear, linear dimensions and masses of samples both before and after testing were measured (Fig. 7). Basing the mass losses, it can be concluded that the wear resistance of the hardest Ti6Al4V-9.7 wt.% Cu alloy increased by 24% compared to the original as-deposited Ti6Al4V alloy. Such an effect can be related to the decrease in the amount of more ductile β-phase resulted from the eutectoid transformation $\beta \rightarrow \alpha(\alpha') + Ti_2Cu$ in samples containing more than 6 wt.% of Cu [17].

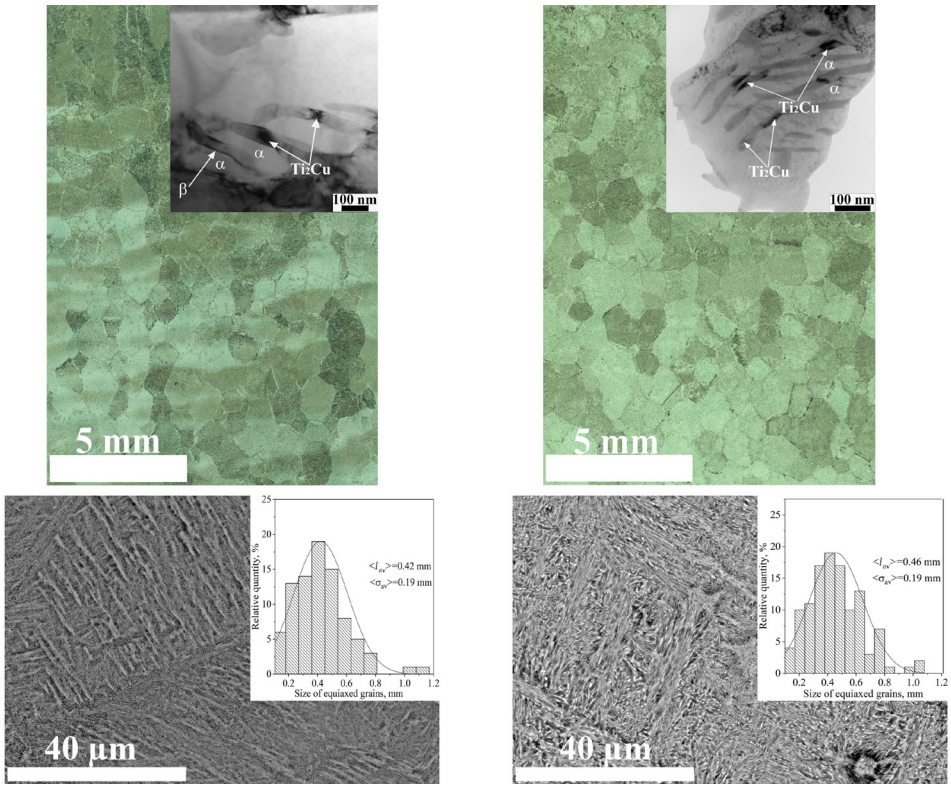


a b

**Fig. 3.** (Color online) Macro- and microstructure, grain size distribution histograms of Ti6Al4V-6 wt.% Cu (a) and Ti6Al4V-9.7 wt.% Cu (b) samples obtained using the electron-beam additive manufacturing.

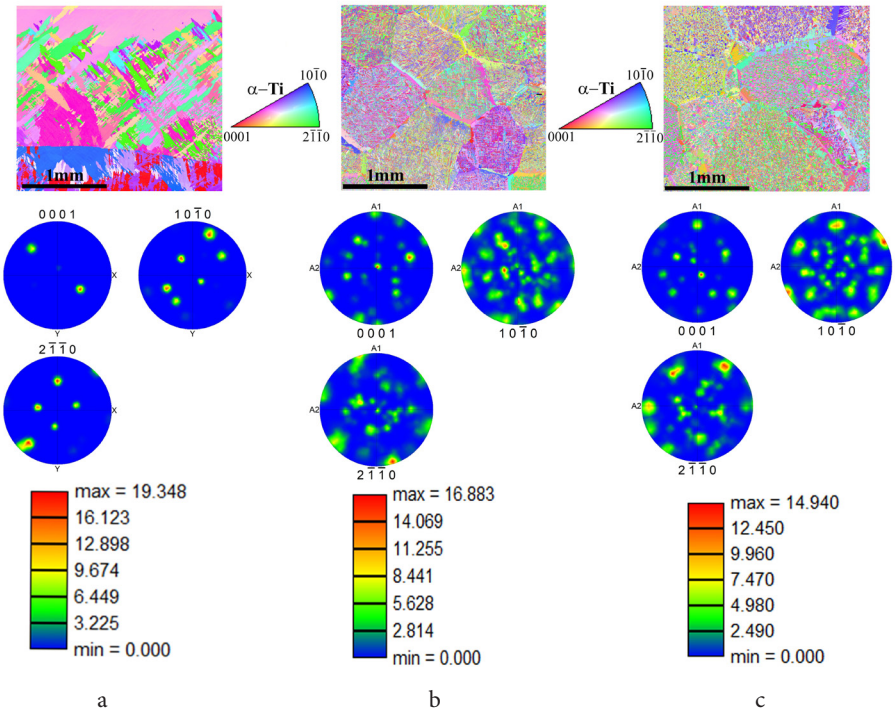


**Fig. 4.** (Color online) Inverse pole figures in the Y direction and pole figures of orientation maps for the middle part of Ti6Al4V-0.6 wt.% Cu (a) Ti6Al4V-6 wt.% Cu (b) Ti6Al4V-9.7 wt.% Cu (c) alloys obtained using the electron-beam additive manufacturing.

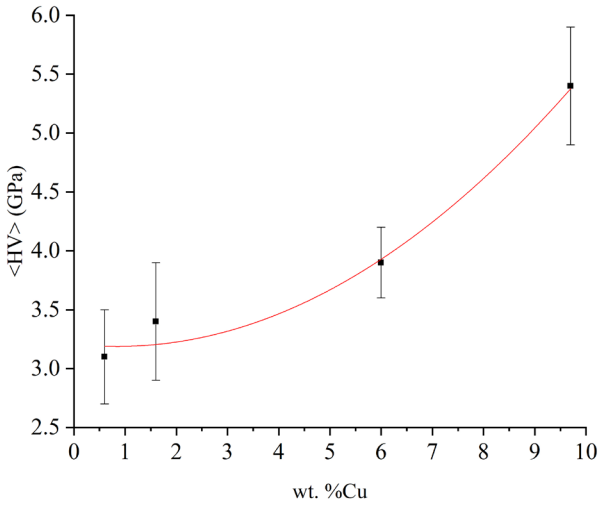


**Fig. 5.** Average value of microhardness of Ti6Al4V-Cu alloys with different copper content obtained by the EBAM method.

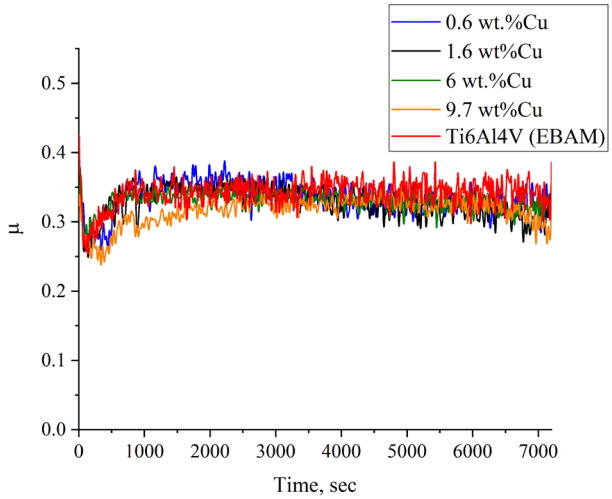


**Fig. 6.** (Color online) Dependence of friction coefficient on sliding time for specimens with different copper content after wear resistance tests on a counterbody made of Ti6Al4V alloy.

The smallest value of linear wear was achieved for samples Ti6Al4V-6 wt.% Cu ($\Delta l = 0.28 \pm 0.01$ mm) and Ti6Al4V-9.7 wt.% Cu ($\Delta l = 0.31 \pm 0.01$ mm), which are 46% and 40% less than the linear wear value for the Ti6Al4V alloy ($\Delta l = 0.52 \pm 0.02$ mm), respectively. This may be due to the formation of thin plates of the α-phase (Fig. 3 a and b), as well as the precipitation of $Ti_2Cu$ intermetallic particles in these alloys, which also have high hardness.

The samples after testing for unlubricated sliding were examined using a scanning electron microscope (SEM) to determine the chemical composition of the worn surface and study the subsurface layer. The SEM images (Fig. 8 a, b, c, Table 1) indicate that the worn surface is represented by areas of different morphology. Agglomerates of particles in Fig. 8 a, b, c pos. 2, 4, 8 were identified as tribo-oxidized wear particles, while relatively smooth surface areas (Fig. 8 a, b, c pos. 1, 3, 5, 6, 7, 9) contain a smaller amount of oxygen and can be attributed to the plastically deformed surface of the alloy. A relatively high content of copper was noted in zone 9, which is a wear particle formed during sliding against a disk and, apparently, containing the $Ti_2Cu$ intermetallic compound. The same particles, but not yet detached from the alloy surface, could be the source of the lower concentration of copper found in zones 7 and 8.

In some areas of the worn surfaces, grooves or cracks are found, indicating that the surface layers of the alloy either were ploughed by abrasive particles, or that the counterbody adhesively interacted with the samples. This interaction is due to the mutual transfer of material from the sample to the counterbody and vice versa. Abrasive wear grooves may

**Table 1.** EDS analysis of Ti6Al4V-Cu samples after wear resistance tests on a counterbody made of Ti6Al4V alloy (Fig. 8).

| Spectrum No | Chemical composition, wt.% | | | | |
|---|---|---|---|---|---|
| | O | Al | Ti | V | Cu |
| 1 | 0.0 | 2.8 | 94.6 | 2.6 | 0.0 |
| 2 | 23.0 | 5.8 | 68.5 | 2.8 | 0.0 |
| 3 | 0.0 | 2.8 | 94.7 | 2.5 | 0.0 |
| 4 | 27.0 | 4.7 | 65.4 | 2.4 | 0.6 |
| 5 | 1.2 | 2.3 | 93.1 | 2.4 | 0.9 |
| 6 | 1.5 | 2.6 | 92.6 | 2.2 | 1.2 |
| 7 | 2.4 | 3.2 | 87.0 | 3.0 | 4.4 |
| 8 | 17.3 | 4.5 | 72.2 | 2.7 | 3.3 |
| 9 | 3.1 | 2.6 | 85 | 2.6 | 6.8 |

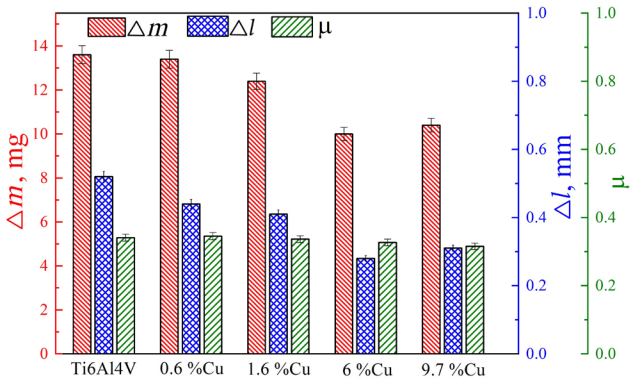


**Fig. 7.** (Color online) Dependence of mass loss, change in length, and COF on copper concentration in Ti6Al4V-Cu samples after wear resistance tests on a counterbody made of Ti6Al4V alloy.

be formed by adhesion pulling out the hard intermetallic particles from the bulk of the metal. Such a particle may then adhere to the counterbody and scratch the surface of the sample. The subsurface layer of Ti6Al4V alloys with different additions of copper was studied by the grazing incidence X-ray diffraction method. A typical X-ray diffraction pattern for Ti6Al4V-Cu samples, which differs only by the intensity of reflections of the $Ti_2Cu$ phase from others is shown in Fig. 8 c. With an increase in the copper concentration, an increase in the concentration of the $Ti_2Cu$ phase and, accordingly, the intensity of this reflection was observed.

Figure 9 shows SEM images of the subsurface layer of the original Ti6Al4V alloy and Ti6Al4V-1.6 wt.% Cu, Ti6Al4V-9.7 wt.% Cu alloys in sections perpendicular to the sliding direction after the sliding wear tests. From Fig. 9 a it can be seen that after sliding friction of the Ti6Al4V sample, a plastically deformed surface layer with a thickness of 22 ± 3 μm formed. This layer is characterized by discontinuous α-Ti plates of different sizes and orientations compared to the structure of the base material. With the addition of 1.6 wt.% copper into Ti6Al4V, a decrease in the thickness of the subsurface layer is observed (Fig. 9 b), and in the Ti6Al4V alloy with a copper concentration of 9.7 wt.%, the deformed layer was not detected at all (Fig. 9 c). The decrease in the plastic deformation penetration is determined by increasing the hardness of the material. In our case, the Vickers hardness was 3.1 ± 0.4, 3.4 ± 0.5 and 5.4 ± 0.5 GPa for titanium alloy samples with copper content of 0.6, 1.6, and 9.7 wt.% Cu, respectively. The level of hardness depended primarily on the proportion of $Ti_2Cu$ particles, thin fragmented α-plates and α' martensite formed as a result of the polymorphic transformation $\beta \rightarrow Ti_2Cu + \alpha(\alpha')$.

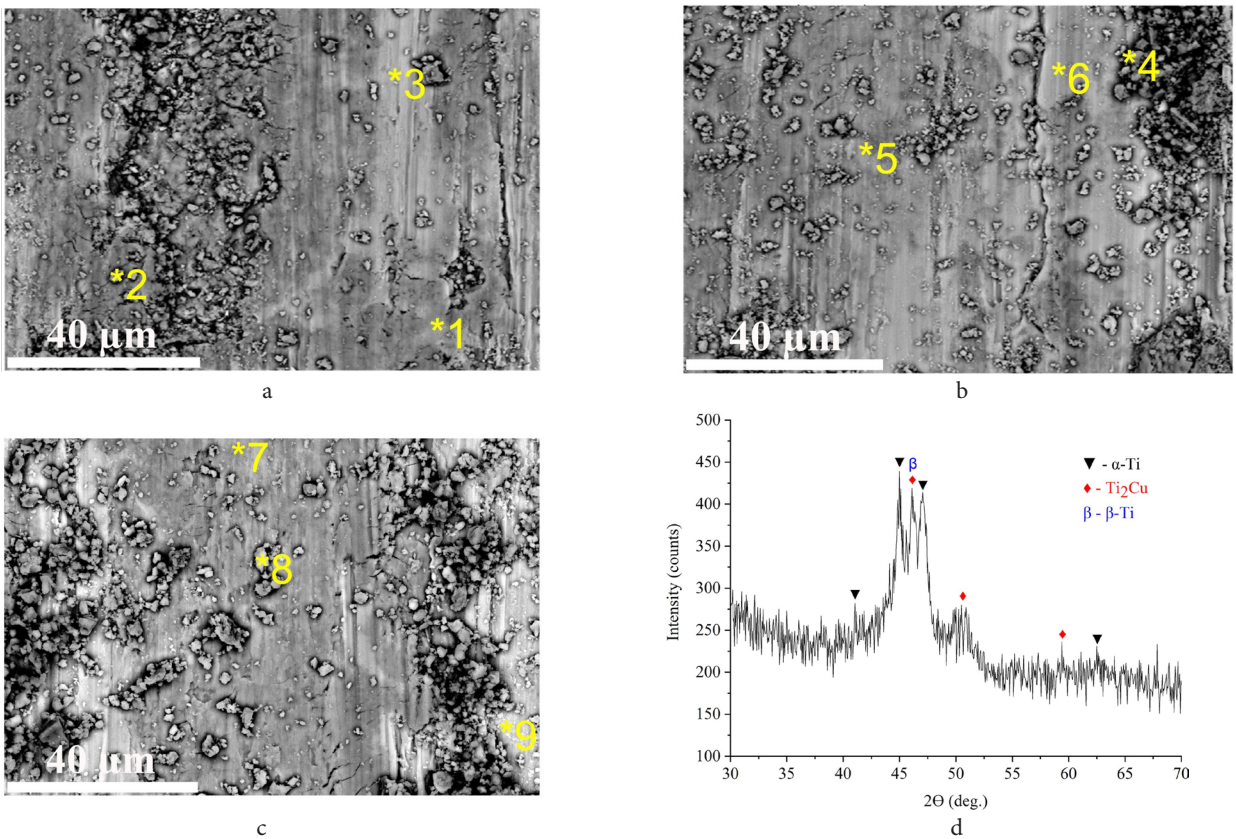


**Fig. 8.** SEM BSE images of the surface after friction of samples Ti6Al4V (a), Ti6Al4V-1.6 wt.% Cu (b), Ti6Al4V-9.7 wt.% Cu (c) and X-ray pattern (d).

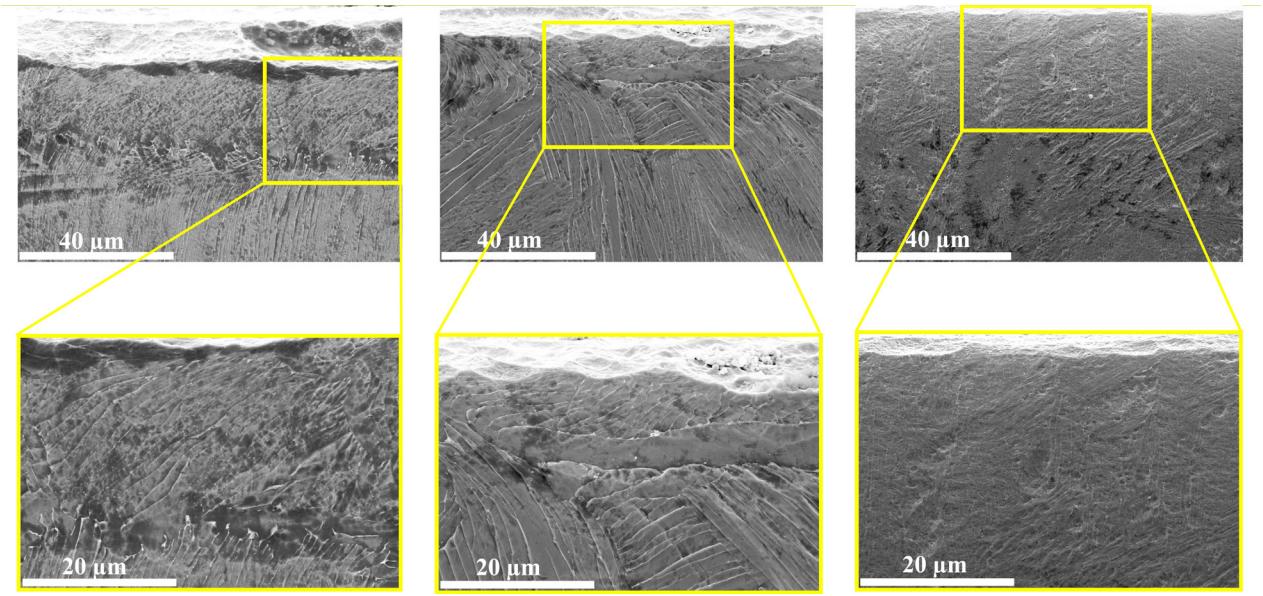


**Fig. 9.** SEM SE images of the subsurface layer of Ti6Al4V (a), Ti6Al4V-1.6 wt.% Cu (b) and Ti6Al4V-9.7 wt.% Cu (c) alloys after wear resistance tests.

## 4. Conclusion

In this work, we studied the effect of alloying titanium alloy Ti6Al4V with copper (0.6, 1.6, 6, 9.7 wt.%) on microhardness and wear resistance of the as-deposited alloys. It has been experimentally established that for all Ti6Al4V-Cu alloys that microhardness grows with the copper contents because copper provides refining the β-grains and consequently α- and α' crystallites as well as hardening of the α-Ti solid solution by $Ti_2Cu$ precipitates.

It is shown that the linear wear values for the Ti6Al4V-6 wt.% Cu and Ti6Al4V-9.7 wt.% Cu alloys are 46% and 40% lower than that of the EBAM Ti6Al4V alloy, respectively, which is due to a decrease in the amount of more ductile β-phase in eutectoid transformation $\beta \rightarrow \alpha\,(\alpha') + Ti_2Cu$ with the addition of copper more than 6 wt.%.

After sliding friction on the EBAM Ti6Al4V alloy, the formation of a plastically deformed subsurface layer with a thickness of 22 ± 3 μm was observed. With an increase in copper concentration in Ti6Al4V-Cu alloys, this tribologically-induced layer became thinner until full disappeared on the hardest sample.

*Acknowledgments. The investigations have been carried out using the equipment of Share Use Centre "Nanotech" of the ISPMS SB RAS. The work was performed according to the Government research assignment for ISPMS SB RAS, project FWRW-2021-0012. The authors thank E.N. Moskvichev and N.L. Savchenko for their help in conducting experimental works.*

## References

1. J.C. Williams, R.R. Boyer. Metals. 10 (6), 705 (2020). Crossref
2. E.A. Kolubaev, V.E. Rubtsov, A.V. Chumaevsky, E.G. Astafurova. Phys. Mesomech. 25 (6), 479 (2022). Crossref
3. A.O. F. Hayama, P.N. Andrade, A. Cremasco, R.J. Contieri, C.R.M. Afonso, R. Caram. Mater. Design. 55, 1006 (2014). Crossref
4. M. Peters, J. Kumpfert, C.H. Ward, C. Leyens. Adv. Eng. Mater. 5 (6), 419 (2003). Crossref
5. M. Millogo, S. Bernard, P. Gillard, F. Frascati. J. Loss. Prevent. Proc. 56, 254 (2018). Crossref
6. F. Yu, H. Wang, G. Yuan, X.Shu. Appl. Phys. A-Mater. 123, 278 (2017). Crossref
7. L. Shao, G. Xie, X. Liu, Y. Wu, J. Yu, K. Feng, W. Xue. Corros. Sci. 190, 109641 (2021). Crossref
8. C. Ohkubo, I. Watanabe, J.P. Ford, H. Nakajima, T. Hosoi, T. Okabe. Biomaterials. 21, 421 (2000). Crossref
9. Y. Geng, S. Konovalov, X. Chen. Usp. Fiz. Met. 21, 26 (2020). Crossref
10. Y. Hu, S. Wu, P. Withers, J. Zhang, H. Bao, Y. Fu, G. Kang. Mater. Design. 192, 108708 (2020). Crossref
11. G. Xian, J. Oh, J. Lee, S. Cho, J.-T. Yeom, Y. Choi, N. Kang. Weld. World. 66 (5), 847 (2022). Crossref
12. J. Lin, Y. Lv, Y. Liu, Z. Sun, K. Wang, Z. Li, Y. Wu, B. Xu, J. Mech. Behav. Biomed. Mater. 69, 19 (2017). Crossref
13. V. Utyaganova, A. Vorontsov, A. Eliseev, K. Osipovich, K. Kalashnikov, N. Savchenko, V. Rubtsov, E. A. Kolubaev. Russ Phys J. 62, 1461 (2019). Crossref
14. N. A. Rosli, M.R. Alkahari, M. F. bin Abdollah, S. Maidin, F.R. Ramli, S.G. Herawan. J. Mater. Res. Technol. 11, 2127 (2021). Crossref
15. X. Peng, L. Kong, J.Y. H. Fuh, H. Wang. J. Manuf. Mater. Process. 5 (2), 38 (2021). Crossref
16. D. Zhang, D. Qiu, M.A. Gibson, Y. Zheng, H.L. Fraser, D.H. StJohn, M.A. Easton. Nature. 576 (7785), 91 (2019). Crossref
17. A.P. Zykova, A.V. Nikolaeva, A.V. Vorontsov, A.V. Chumaevskii, S.Yu. Nikonov, E.N. Moskvichev, D.A. Gurianov, N.L. Savchenko, E.A. Kolubaev, S.Yu. Tarasov. Phys. Mesomech. 25 (6), 5 (2022). (in Russian) Crossref